Dynamic Pulmonary SPECT of Xenon-133 Gas Washout

Kazuyoshi Suga, Kazuya Nishigauchi, Norihiko Kume, Shinji Koike, Katsuyuki Takano, Osamu Tokuda, Tsuneo Matsumoto and Naofumi Matsunaga

Department of Radiology, Yamaguchi University School of Medicine, Ube, Yamaguchi, Japan

A triple-detector SPECT data acquisition mode of "continuous repetitive rotation acquisition" was applied to dynamic pulmonary SPECT with ^{133}Xe gas. **Methods:** Subjects included 7 healthy volunteers, 22 patients with a space-occupying mass lesion, 22 with obstructive lung disease and 10 with restrictive lung disease. Following rebreathing of ^{133}Xe, equilibrium and washout SPECT images during spontaneous breathing were acquired every 30 sec for 5–7 min. Regional ^{133}Xe washout was assessed by the real half-time ($T_{1/2}$) and mean transit time (MTT) images. **Results:** SPECT and MTT images represented a gravity-induced gradient of ventilation in normal lungs and detailed the distribution of heterogeneous ^{133}Xe washout in patient's lungs with or without abnormalities on chest x-ray CT. The $T_{1/2}$ (111.4 ± 26.4 sec) and its coefficient of variation (0.36 ± 0.13) in obstructive lung diseases were significantly different from those (56.8 ± 3.9 sec and 0.16 ± 0.15) in restrictive lung diseases ($p < 0.001$, $p < 0.05$, respectively). Comparison of SPECT and planar studies assessed in 19 patients revealed superiority of SPECT in detecting ventilatory abnormalities and a high correlation of $T_{1/2}$ between the two studies ($r = 0.977$, $p < 0.001$). **Conclusion:** This modality has excellent potential for elucidating the distribution and nature of ventilatory abnormalities.

Key Words: SPECT; dynamic study; xenon-133 gas; lung ventilation

J Nucl Med 1996; 37:807–814

Pulmonary washout study with ^{133}Xe gas is widely used to detect regional changes of ventilation in both large and small airways (*1–19*). With planar imaging, however, it is difficult to obtain multidirectional views, and its two-dimensional character inherently limits its sensitivity and accuracy because of overlapping of ^{133}Xe activity between lesions and normal lungs and effects of ^{133}Xe on the chest wall (*1,2,7*). Tomographic imaging is necessary for more sensitive and accurate estimation of regional ventilation abnormalities. Notwithstanding, earlier single-detector, SPECT systems failed to effectively visualize the dynamic process of ^{133}Xe washout because of limited capability in short-time acquisition of data (*14*).

A high sensitive SPECT system with rapid data acquisition capacity could be an appropriate modality for imaging temporal changes of ^{133}Xe washout. One technical solution is the use of a multidetector SPECT system with continuous repetitive rotation acquisition (CRRA) mode (*20–28*). This technique is suitable for obtaining dynamic SPECT of those organs in which change or elimination of radioactive tracer is relatively fast, and it can reduce qualitative and quantitative effects of tracer clearance on image quality (*20*). In fact, recent studies using this technique represented high-quality dynamic images of the myocardium with teboroxime (*21*) and the brain with [^{123}I]-iodoamphetamine (*25*) without significant quantitative errors.

In this study, we attempted dynamic pulmonary SPECT of ^{133}Xe washout using a triple-detector SPECT system with CRRA mode and evaluated its potential to assess regional ventilatory abnormality.

Received Mar. 27, 1995; revision accepted Oct. 8, 1995.

For correspondence or reprints contact: Kazuyoshi Suga, MD, Department of Radiology, Yamaguchi University School of Medicine 1144, Kogushi, Ube 755, Japan.

MATERIALS AND METHODS

Subjects

We studied seven healthy, nonsmoking volunteers (7 men; aged 25–40 yr) with normal ventilatory function test and chest radiograph findings and 54 patients (35 men, 19 women; aged 35 to 78 yr), including 22 patients with a space-occupying mass lesion (17 with lung cancer and 5 with silicosis), 22 patients with obstructive lung disease [13 with pulmonary emphysema, 4 with bronchial asthma, 3 with chronic bronchitis and 2 with diffuse panbronchiolitis (DPB)] and 10 patients with restrictive lung disease [6 with usual interstitial pneumonitis (UIP) and 1 each with desquamative interstitial pneumonitis, alveolar proteinosis, hypersensitivity pneumonitis and lung fibrosis due to systemic lupus erythematosus]. Informed consent was obtained from all participants.

Of the 17 patients with lung cancer, 9 had adenocarcinoma, 5 had squamous-cell carcinoma, 2 had small-cell carcinoma and 1 had large-cell carcinoma. The lesion size ranged from 21 to 55 mm in diameter. Nine patients had a central-type tumor located in the hilum, and the remaining eight had a peripheral-type tumor in the peripheral lung adjacent to the pleura. All five patients with silicosis had large opacities ranging in size from 21 to 67 mm in the upper and middle lungs, accompanied with diffusely distributed small opacities.

Dynamic SPECT

Dynamic SPECT was performed using a triple-detector SPECT system, in which three detectors surround the imaging field triangularly. Each detector has a rectangular field of view (the effective field of view is 38 × 21 cm), and the radius of rotation is adjusted by radial translation. Data were recorded with a low-energy, high-resolution collimator. FWHM obtained by a line source within an acrylic phantom with a radius of 20 cm, which contained ^{133}Xe gas of a concentration of 60 MBq/liter, was 12.8 mm at the center of the phantom and 9.7 mm at 6 cm from the center. The detector system was interfaced to dedicated nuclear medicine computers.

Each subject, in a supine position on the gantry, put on a mask connected to the ^{133}Xe gas control system to ensure a constant inspiratory concentration of ^{133}Xe gas (60–72 MBq/liter) with oxygen. After 6 min of closed circuit inhalation of ^{133}Xe gas, dynamic SPECT acquisition began, with 64 × 64 matrices and an energy window of 80 keV ± 20%. Subjects breathed spontaneously throughout the acquisition.

Dynamic data acquisition was performed with the return mode of the CRRA. To eliminate the settling time between projections and acquisition of multiple temporal samples of data, each detector was continuously and repeatedly rotated in the clockwise (for 15 sec) and counterclockwise (for 15 sec) directions across the same projection arc, and back again. With the use of three detectors, a gantry rotation of 120° around the chest provided projections over a full 360° arc. To minimize scanning time, we used a continuous acquisition with data divided into projection images at 6° intervals rather than the more conventional step-and-shoot approach

(*20,21*). The projection data for an equilibrium image were initially acquired during closed circuit inhalation of ^{133}Xe gas for 30 sec, and subsequently a total 10–14 sets (total, 5–7 min) of the projection data (one per 30 sec) for washout imaging were acquired during open circuit inhalation.

Image Processing

Serial transaxial and coronal equilibrium and washout SPECT images were reconstructed by filtered backprojection with a ramp filter after preprocessing with a Butterworth filter (a cutoff frequency of 0.13 cycles/cm, order 8) from the dynamic acquisition data. The slice thickness was 1 pixel (3.2 mm). Neither attenuation correction nor scatter correction was performed, because these corrections were considered to be unnecessary since only rates of change of ^{133}Xe gas was being measured. Averaged projection data at same angle in both clockwise and counterclockwise rotations was used for the reconstruction of a single SPECT image. Therefore, elimination of ^{133}Xe during the acquisition time of 30 sec was averaged.

Evaluation of SPECT Images

Visual evaluation of SPECT images was performed by three nuclear medicine specialists experienced in ^{133}Xe ventilation studies. The interpreters were blinded as to the diagnosis and visually assessed the presence or absence of abnormal ^{133}Xe retention by comparison with the SPECT images in the normal subjects. Then,

TABLE 1
Comparison between SPECT and Planar Studies

Patient no.	Age (yr)	Sex	Diagnosis (Histology)	Lesion sites on chest x-ray CT (mm)	Abnormal retention sites on SPECT	$T_{1/2}$ in the abnormal retention sites (sec)	
						SPECT	Planar
1	63	M	Lung cancer (Sq)	Rt-hilum (45 × 43)	Rt-S6	107.0	98.4
2	63	M	Lung cancer (Small)	Rt-hilum (35 × 34)	Rt-lower lobe	156.7	145.4
3	73	F	Lung cancer (Small)	Lt-hilum (45 × 35)	Lt-upper lobe	103.4	95.4
4	69	M	Lung cancer (Sq)	Rt-S4 (55 × 50)	Lt-upper lobe	84.0	Not detected
5	63	M	Lung cancer (Ad)	Lt-S5 (30 × 25)	Neighboring the tumor	63.2	Not detected
6	68	M	Lung cancer (Large)	Rt-S10 (53 × 43)	Neighboring the tumor	74.0	65.1
7	68	M	Silicosis	Large opacities in both upper lungs with diffuse small opacities	Rt-upper lobe	83.3	Not detected
					Lt-upper lobe	87.5	78.4
					Lt-lower lobe	85.1	75.4
8	78	M	Emphysema	Both-upper lobes	Rt-upper lobe	142.5	120.5
					Lt-upper lobe	132.5	125.4
9	76	M	Emphysema	No abnormal findings	Rt-upper lobe	117.3	112.6
					Rt-middle lobe	103.5	98.9
					Lt-upper lobe	92.4	88.5
10	63	F	Chr. bronchitis with bronchiectasis	Diffusely	Rt-upper lobe	217.6	207.8
					Lt-upper lobe	178.5	160.4
					Rt-middle lobe	107.5	99.2
					Lt-lingula lobe	90.7	80.3
11	76	F	Chr. bronchitis with bronchiectasis	Lt-lower lobe	Lt-lower lobe	100.5	90.3
12	35	M	DPB	Both mid & lower lungs	Rt-middle lobe	134.4	Not detected
					Lt-lingula lobe	103.5	Not detected
					Rt-lower lobe	158.4	112.3
					Lt-lower lobe	145.5	119.6
					Outer lung zones	154.0	Not detected
					in both lower lungs	150.6	Not detected
13	42	M	DPB	Both mid & lower lungs	Rt-lower lobe	175.3	140.3
					Rt-lower lobe	121.5	98.7
					Outer lung zones	141.0	Not detected
					in both lower lungs	135.3	Not detected
14	66	F	UIP	Diffusely	Not detected	(61.2)*	(54.2)*
15	64	M	UIP	Both mid & lower lungs	Not detected	(57.5)*	(53.1)*
16	47	M	UIP	Dorsal sites of both lower lungs	Not detected	(65.6)*	(56.3)*
17	41	M	Alveolar proteiniosis	Both mid & lower lungs	Not detected	(48.6)*	(46.4)*
18	48	F	Bronchial atresia	Rt-S4	Rt-S4	47.3	Not detected
19	41	M	Giant bullae (120 × 87)	Rt-upper lobe	Rt-upper lobe	143.5	131.2

*Four patients with restrictive lung disease (14–17) have no retention. $T_{1/2}$ is estimated in the lung lesions on chest x-ray CT.

Sq = squamous-cell carcinoma; Ad = adenocarcinoma; Small = small-cell carcinoma; Large = large-cell carcinoma; DPB = diffuse panbronchiolitis; UIP = usual interstitial pneumonia.

SPECT findings were compared with chest x-ray CT scans. In some subjects combined with thin-slice, high-resolution imaging.

Quantitative Analysis

In the investigation of whether quantitative analysis can be applicable to dynamic SPECT, the real half-time ($T_{1/2}$) of lung regions, defined as the clearance time required to reach the 50% level of equilibrium count rate during washout, was assessed on transaxial SPECT images. In normal subjects, a square 7 × 7-pixel region of interest (ROI) was symmetrically placed over both the ventral and dorsal portions near the pleura at the three zones of the upper, middle and lower lungs (at the aortic arch, at the hilum and just above the diaphragm, respectively). In patients, ROIs larger than 9 pixels were placed manually over ^{133}Xe retention sites or lesions on chest x-ray CT, as well as over non-^{133}Xe retention sites or nonlesion sites in the ventral and dorsal portions at the three lung zones. Outline of retention sites was determined on the 2.5-min washout image because normal subjects did not demonstrate any abnormal retention beyond the 2-min images. Simultaneously, the background was outlined between the lungs (overlying the vertebrae) using a square 5 × 5-pixel ROI, and the ^{133}Xe washout curve was corrected for background by subtracting the average counts per pixel in the background from those in the lung regions throughout washout phase. For each lung region, $T_{1/2}$ was taken as an average of two or three measurements, including adjacent sections just above and/or below.

In addition, to assess heterogeneity of ^{133}Xe washout, we compared the coefficient of variation (CV) of $T_{1/2}$ for the volunteers with that for the patients with obstructive and restrictive lung diseases. The $T_{1/2}$ of each square 3 × 3-pixel ROI was acquired throughout the entire lungs on the coronal section SPECT image at the center of the mediastinum and the CV of the $T_{1/2}$ was calculated for each subject.

Furthermore, we developed a functional mean transit time (MTT) image, which displays the MTT with a gray scale. Transaxial outlined lung regions were initially obtained from the equilibrium image. On the basis of the height over area method, the ratio of the equilibrium count rate to the sum of the counts obtained during washout (corrected for the background as mentioned above), which yields the MTT value, was computed automatically for every pixel in the outlined lungs (*2,29,30*). The gray scale of each pixel was made proportionate to the magnitude of MTT on the functional image. Because of the present limitations of our nuclear medicine computer, output for the absolute MTT value for each pixel was not available.

Comparative Study of SPECT and Planar Imaging

A comparative study of SPECT and planar ^{133}Xe imaging was performed in 6 of the 7 volunteers and in 19 patients, including 17 patients selected from the above 54 patients, 1 with bronchial atresia and 1 with giant bullae (Table 1). A planar study was performed 7–20 days after the SPECT study. All patients had chronic and/or stable lung disorders and did not show any changes in both chest radiographs and ventilatory function test during the interstudy period (Table 1). Each subject, in a supine position, inhaled ^{133}Xe gas in the same manner as the SPECT study. An equilibrium image was acquired in the posterior projection by collecting 100K counts and subsequent washout images were obtained at 30-sec intervals for 5–7 min. In normal subjects, a square 7 × 7-pixel ROI was symmetrically placed over the central lung fields in the three lung zones of both lungs. In patients, similarly to the SPECT study, ROIs were placed over retention sites or lesions on chest x-ray CT/radiograph, as well as over non-^{133}Xe retention sites or nonlesion sites at the three lung zones. The outline of retention was determined on the 2.5-min washout images. Washout curves were corrected by subtracting the average counts/pixel derived from the background region (5 × 7 pixels, overlying the lower thoracic and upper lumbar vertebrae) between and below the lungs.

Xenon-133 retention sites were enumerated separately for the two studies and the detection capacities of retention were compared. Furthermore, $T_{1/2}$ values in the abnormal lung regions with retention were compared.

In addition, a comparison between the planar image and summed coronal SPECT image reconstructed by all coronal SPECT sections was performed. In single-direction planar imaging, ^{133}Xe washout in a lung lesion is considered to be inevitably influenced by fast washout of overlapping normal lungs or different washout of other overlapping lesions (*1–4*). In contrast, cross-section SPECT removes such tissue cross-talk in ^{133}Xe washout. To compare $T_{1/2}$ in the same condition as planar imaging, summed SPECT images having tissue cross-talk are considered to be more adequate. Moreover, this image that shows the same appearance in contour as the planar image allows easier comparison of images and permits placement of same-sized ROIs over the same lung regions as in the planar image. ROI placement and background correction were performed similarly to that in planar study; $T_{1/2}$ was also compared.

Statistical Analysis

Data for $T_{1/2}$ and CV of $T_{1/2}$ were presented as mean values ± s.d. Statistical analysis was performed by Student's t-testing. A probability value of less than 0.05 was considered statistically significant.

RESULTS

Normal Subjects

Equilibrium SPECT image in the volunteers showed homogeneous ^{133}Xe activity throughout the entire lungs, indicating that ^{133}Xe activity reached equilibrium. The sequence of washout images did not show any clear artifacts caused by changing distribution of ^{133}Xe. Moreover, the early images revealed that ^{133}Xe washout was faster in the dependent (dorsal) lungs than in the independent (ventral) lungs (Fig. 1). On the later washout images, (beyond 2 min), ^{133}Xe activity disappeared homogeneously from the entire lungs without any abnormal retention. On the MTT image, the relatively prolonged washout in the independent lungs was also noted (Fig. 1). The $T_{1/2}$ in the dependent lungs was significantly shorter than that in the independent lungs in all three zones ($p < 0.01$), with an average difference of 6.4 ± 3.2 sec (Table 2). When all data from all lung zones in seven volunteers were combined, the mean $T_{1/2}$ was 48.4 ± 4.3 sec, and the mean CV of $T_{1/2}$ was 0.08 ± 0.03.

Patients

All 22 patients with a space-occupying mass showed defective ^{133}Xe activity corresponding to the mass on the equilibrium image (the smallest size was 21 mm). In addition, reduced ^{133}Xe activity in the lung distal to the mass was observed in all five patients with silicosis and in six of nine with a central-type lung cancer. On the washout image, all 22 patients except 2 with peripheral small-cell lung cancer showed ^{133}Xe retention in the lung distal to the mass. The MTT image also showed prolonged MTT in these sites (Fig. 2). In addition to retention adjacent to the mass, other retention was seen in the remaining lungs in 12 of 17 patients with lung cancer and in all 5 patients with silicosis. In these sites, emphysematous change or bronchovascular bundle thickening was observed on chest x-ray CT. Nine patients with central-type lung cancer showed more intensive and prolonged retention compared to the 8 patients with peripheral-type tumors. The $T_{1/2}$ in the retention site in the former group (228.1 ± 134.2 sec) was significantly longer than that (73.7 ± 8.4 sec) in the latter group ($p < 0.01$).

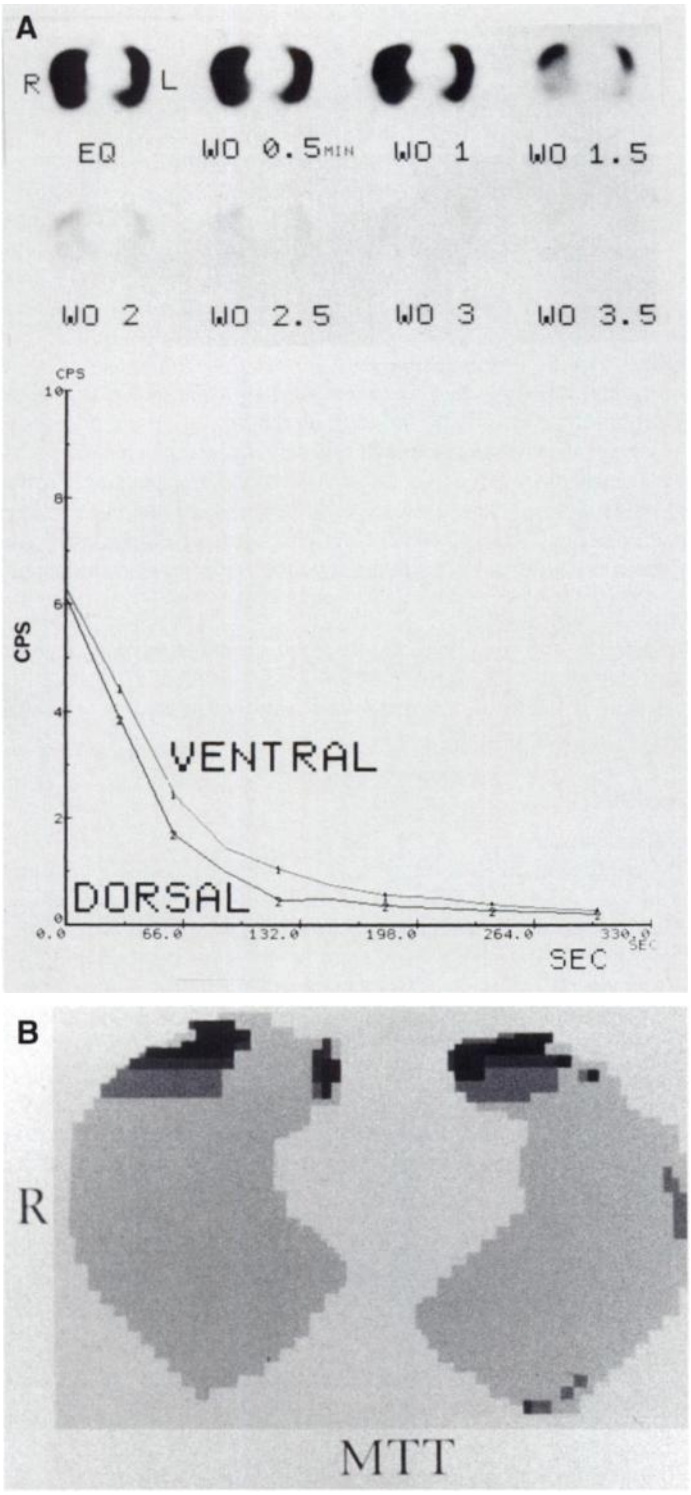

FIGURE 1. (A) Sequence of transaxial equilibrium and washout (0.5–3.5 min) SPECT at lower lung level in a volunteer (above). Early washout images (0.5–2.0 min) show greater ^{133}Xe activity in ventral than dorsal portion. Washout curves in right lung reveal that $T_{1/2}$ (53.5 sec) in ventral portion is longer than dorsal portion (42.8 sec) (bottom). (B) MTT image shows prolonged MTT in ventral portions (greater MTT magnitude is reflected by darker pixel color.).

All 22 patients with obstructive lung disease showed multiple ^{133}Xe retention, which was frequently seen even on the late (5–6 min) washout images (Figs. 3–5). The MTT image showed more heterogeneous distribution of MTT compared to normal subjects and patients with restrictive lung disease (Figs. 3–5). Xenon-133 retention was seen more extensively than the spread of lesions visible on chest x-ray CT in 5 of 13 patients with pulmonary emphysema, 3 with chronic bronchitis and 2 with DPB. Although 2 of 13 patients with pulmonary emphysema and 2 of 4 with bronchial asthma did not show any abnormal opacities or radiolucencies throughout the lungs on chest x-ray CT, retention was noted. Two patients with DPB showed characteristic symmetrical retention in the outer zone of both lungs (Fig. 5). Retention sites showed diminished ^{133}Xe activity on the equilibrium images in severe bronchiectatic lesions in three patients with chronic bronchitis and one with bronchial asthma, indicating diminished washin of ^{133}Xe (Fig. 3). In 22 patients, $T_{1/2}$ in retention site (136.2 ± 37.8 sec) was significantly longer than that (84.5 ± 14.2 sec) in the lungs without retention ($p < 0.01$), and the combined $T_{1/2}$ (111.4 ± 26.4 sec) for both sites was significantly longer than the seven volunteers ($p < 0.001$) (Table 2). Moreover, $T_{1/2}$ (93.2 ± 20.5 sec) in the lung areas without any abnormalities on chest x-ray CT in 15 patients was also significantly longer than that in the seven subjects ($p < 0.001$). The mean CV of $T_{1/2}$ (0.36 ± 0.13) in 22 patients was significantly higher than that in the subjects ($p < 0.01$).

TABLE 2
Comparison of $T_{1/2}$ between Ventral and Dorsal Lung Portions in Seven Subjects

Lung zones	Mean $T_{1/2}$ ± s.d. (sec)	
	Ventral	Dorsal
Upper	53.5 ± 2.3	47.4 ± 3.4
Middle	52.5 ± 3.8	43.8 ± 2.7
Lower	51.4 ± 4.3	42.1 ± 4.0

$T_{1/2}$ in dorsal portion is significantly shorter than ventral portion in all three lung zones ($p < 0.01$, respectively).

In contrast to the obstructive lung diseases, none of the 10 patients with restrictive lung disease showed any significant retention on the washout image, and the MTT image disclosed less heterogeneity in MTT distribution. The $T_{1/2}$ in the affected lung (56.4 ± 4.2 sec) was not statistically different from that (57.3 ± 3.7 sec) in the unaffected areas. The combined $T_{1/2}$ (56.8 ± 3.9 sec) for both lung areas was significantly faster than the mean $T_{1/2}$ (111.4 ± 26.4 sec) in the patients with obstructive lung diseases ($p < 0.001$) (Table 3). The mean CV of $T_{1/2}$ (0.16 ± 0.15) was not different for the subjects ($p = 0.154$) but was significantly lower than the obstructive lung diseases ($p < 0.05$).

Comparative Study of SPECT and Planar Imaging

In the planar study of six subjects, the difference in ^{133}Xe washout between the dorsal and ventral lungs was not recognized. The mean $T_{1/2}$ (38.8 ± 2.9 sec) in the three lung zones was significantly faster than that (46.6 ± 3.1 sec) of the SPECT images ($p < 0.01$). The mean percent change of ^{133}Xe activity defined as

$$\frac{[(\text{count rate at 30 sec following washout}) - (\text{initial count rate before washout})]}{(\text{initial count rate before washout})} \times 100\%$$

was 28.6% ± 3.9%.

Of the 31 ^{133}Xe retention sites seen on the SPECT images of 19 patients, 10 were not detected or indistinct on planar image (Table 1). Moreover, in correlation with chest x-ray CT, SPECT detailed the distribution of retention anatomically. For instance, segmental or lobar retention in the patients with lung cancer were more clearly depicted on SPECT images. Symmetrical

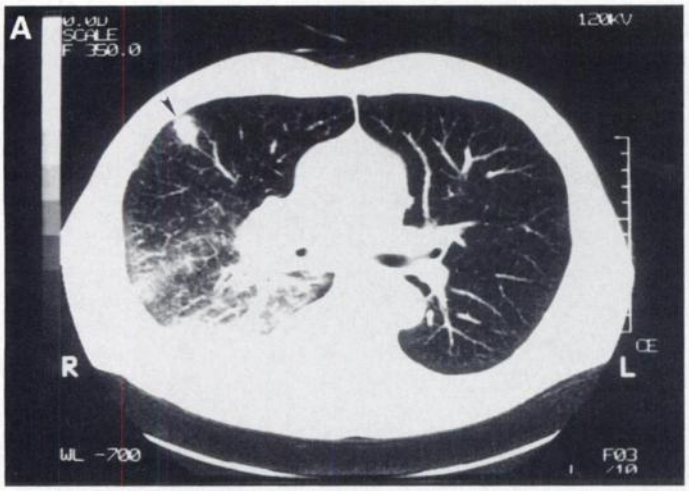

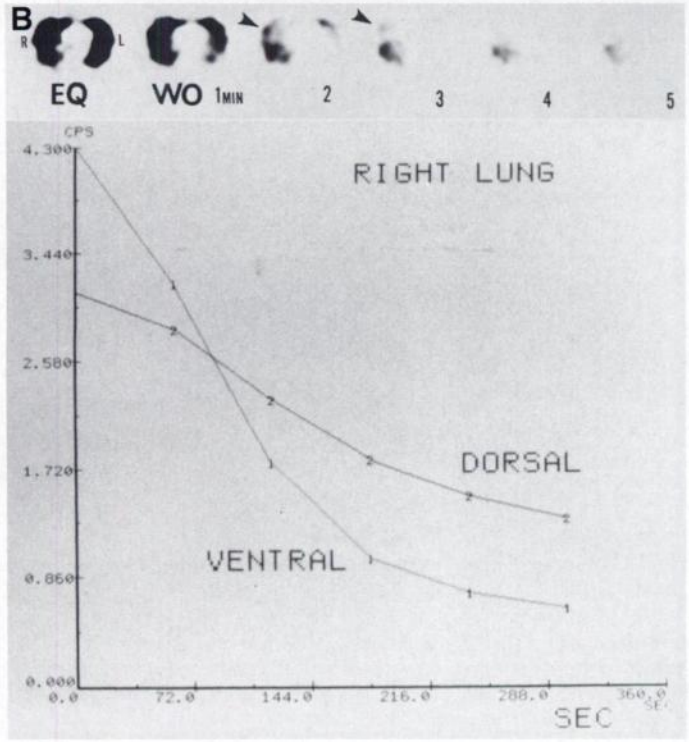

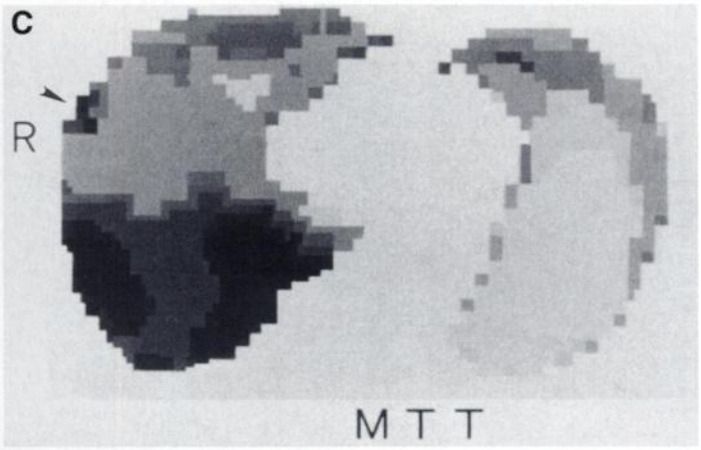

FIGURE 2. (A) Chest CT scan from a 63-yr-old man with lung cancer shows a right hilar tumor with secondary change in right lower lobe and an inflammatory small opacity in middle lobe (arrowhead). Fiberoptic bronchoscopy shows stenosis in lower and middle lobe bronchi. (B) SPECT shows ^{133}Xe activity on equilibrium image and prolonged ^{133}Xe washout in right lower lobe. Retention is also seen near the small opacity (arrowheads) (above). Washout curves in right lung show more prolonged $T_{1/2}$ (222.9 sec) in dorsal portion than ventral portion (104.7 sec) (bottom). (C) MTT image shows prolonged MTT in right dorsal portion and near the small opacity (arrowhead).

retention of the outer lung zones in two patients with DPB (Fig. 5) and segmental retention in the distal lung of obstructed bronchus in the patient with bronchial atresia were visible by SPECT alone. The $T_{1/2}$ (128.8 ± 44.9 sec) in 27 abnormal lung regions, with retention on SPECT images, (excluding four regions with retention in the outer lung zones in two patients with DPB) was significantly longer than that (104.0 ± 36.2 sec) in the corresponding regions on the planar image ($p < 0.001$). When using $T_{1/2}$ data in normal subjects, the difference in $T_{1/2}$ (82.2 sec) between these regions and normal lungs on SPECT images was greater than that (65.2 sec) in the planar study.

When comparing $T_{1/2}$ in 21 retention sites seen on the summed coronal SPECT and planar images (Table 1), the value of SPECT (125.8 ± 36.9 sec) was significantly longer than that (107.2 ± 26.1 sec) of planar study ($p < 0.001$). The $T_{1/2}$ (70.6 ± 15.6 sec) of summed SPECT in 68 lung regions without retention in the three lung zones (including four lung lesions in four patients with restrictive lung disease) was also significantly longer than that (60.0 ± 16.1 sec) of the planar study ($p < 0.01$). The $T_{1/2}$ in the lung regions with and without ^{133}Xe retention acquired by summed SPECT showed high correlation with those acquired by the planar study ($r = 0.977$, $p < 0.001$) (Fig. 6).

DISCUSSION

Dynamic SPECT acquired using the CRRA mode provided good image quality without noticeable artifacts, despite relatively rapid changes of ^{133}Xe activity in the lung. A recent phantom study of dynamic SPECT imaging suggested that distortion of SPECT image was not noticeable and its resolution was scarcely degraded if the percent change of tracer activity remained within 20%–50% during the acquisition time (*20,23–25,27,28*). In this study, the percent change of ^{133}Xe activity during the initial fast phase of ^{133}Xe washout measured by the planar image in the normal lungs was 28.6% ± 3.9%, indicating that the acquisition time of 30 sec is applicable for dynamic SPECT in normal subjects and in patients with slower ^{133}Xe washout.

The SPECT images in this study effectively visualized the dynamic process of pulmonary ^{133}Xe washout on the cross-section image, detected ^{133}Xe retention in patient's lungs more sensitively and detailed anatomically the distribution of ^{133}Xe retention than the planar images. Faster washout in the dependent lungs than the independent lungs in normal subjects is considered to reflect a gravity-induced gradient of ventilation (Fig. 1, Table 2). Intrapleural pressure gradients and the size of the alveoli at end-expiration are influenced by lung weight, so that air flow and ventilatory turnover rate are greater in the dependent lungs (*2,13,14,18,31*).

In obstructive lung disease, SPECT frequently showed more extensive ^{133}Xe retention than the spread of lesions visible on chest x-ray CT and retention/washout delay, even in the lungs without any abnormalities on x-ray CT. These findings seem to reflect early obstructive changes in the small airways. In obstructive lung disease, early pathological changes are predominantly localized to small, distal airways and structural changes strongly affect airway resistance and airflow rates per unit lung volume, which results in significant ^{133}Xe washout delay (*1,2,9,12–14*). Xenon-133 washout study is more sensitive in the early detection of such ventilatory abnormalities in the small airways than ^{81m}Kr study under steady-state condi-

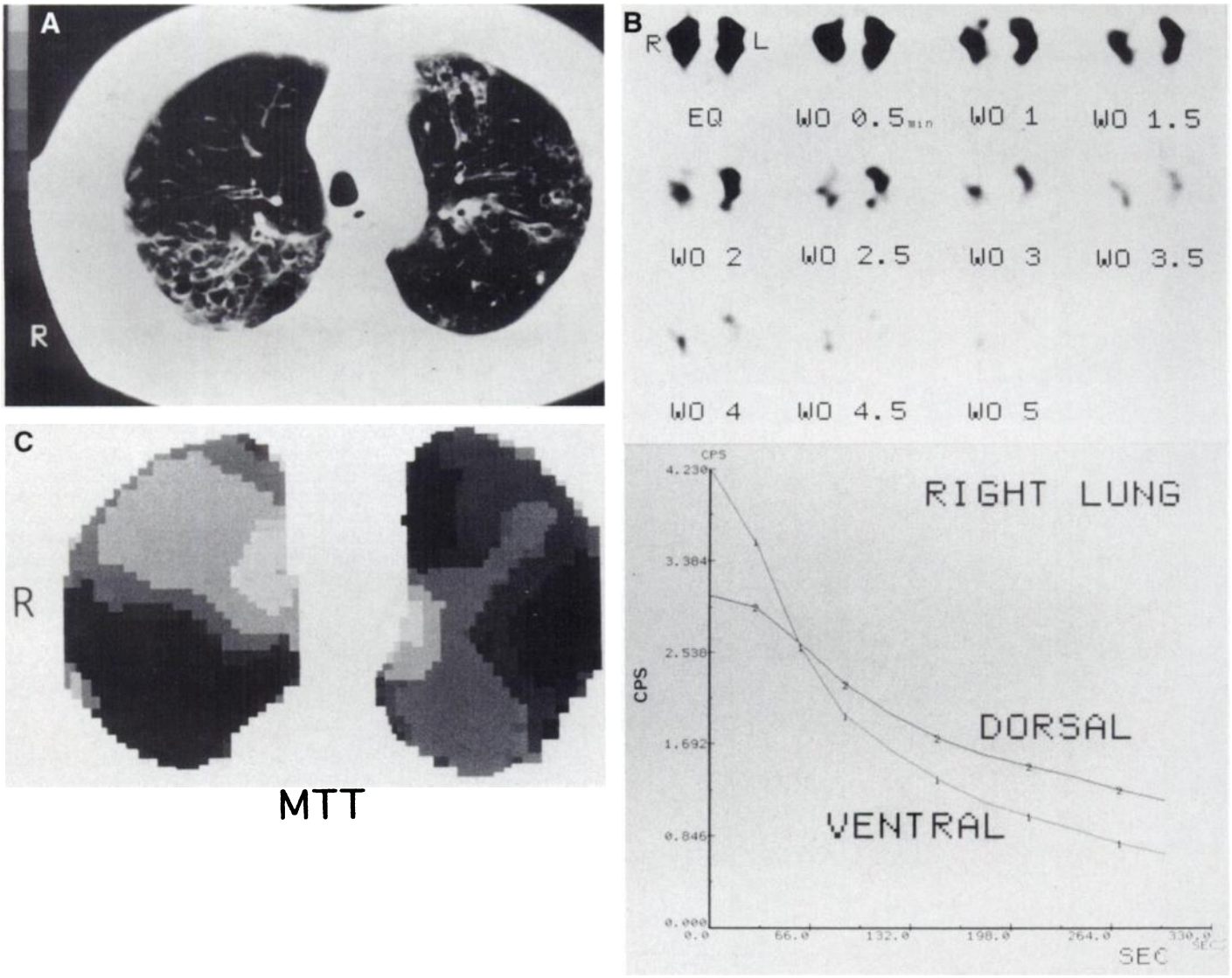

FIGURE 3. (A) Chest CT scan from a 63-yr-old woman with chronic bronchitis shows bronchiectasis in both upper lobes, while the change is slight in the right ventral portion. (B) SPECT shows heterogeneous washout in both lungs (top). Washout curves in right lung show more reduced initial ^{133}Xe activity and more prolonged $T_{1/2}$ (222.9 sec) in dorsal portion with severe bronchiectasis than the ventral portion (81.7 sec) (bottom). (C) MTT image shows heterogeneously prolonged MTT, which is more prolonged in the right dorsal than ventral portion.

tions (*6,8,14*). Previous chest x-ray CT/pathology correlation studies revealed x-ray CT to be mildly insensitive to obstructive lung disease (*12,32,33*). Symmetrical retention in the peripheral outer lung zones in DPB patients suggests a difference in susceptibility to obstructive changes between the inner and outer lung zones due to pathologic features in the walls of respiratory bronchiole (*13,14,34*) (Fig. 5). The capacities of cross-section SPECT for detecting retention are apparently greater than planar studies, since planar imaging inherently has overlapping ^{133}Xe activity of other lung lesions or normal lungs. Thus, cross-section SPECT appears more sensitive and reliable than chest x-ray CT or ^{133}Xe planar studies for early detection of ventilatory abnormalities in obstructive lung disease.

Cross-section SPECT demonstrated differences in ventilation abnormalities between obstructive and restrictive lung diseases (Table 3). In restrictive disease, airway patency is usually maintained, although the airway is slightly reduced. Therefore, washout rates are not significantly prolonged because of the predominance of decreased compliance over airway resistance (*1,2,12,13*).

In space-occupying mass lesions, SPECT had greater sensitivity for detecting ^{133}Xe retention than the planar study. Moreover, SPECT results were more easily comparable with chest x-ray CT than planar imaging and offered better localization of ventilation abnormalities related to the mass (Fig. 2). Reduced ^{133}Xe activity on the equilibrium image and ^{133}Xe retention on the washout image in the lungs distal to the mass may reflect poor washin and prolonged washout of ^{133}Xe gas due to disturbed ventilation caused by stenosis and/or obstruction of bronchi induced by the mass (*2,15*). In fact, in all six patients with a central-type lung cancer who showed reduced ^{133}Xe activity on the washout image, obstructive or stenotic changes in the corresponding bronchus were verified by fiberoptic bronchoscopy. The more intensive and prolonged retention in central-type than peripheral-type lung cancer may reflect the difference of degree of the effects of the mass on bronchi between the two groups.

Quantitative approaches using $T_{1/2}$ and the MTT image seem to be applicable to the present modality because these methods revealed a gravitational effect of ventilation in normal lungs, as well as greater heterogeneity of ^{133}Xe washout in obstructive lung diseases than restrictive lung diseases. Such quantification should be used together with visual assessment to clarify

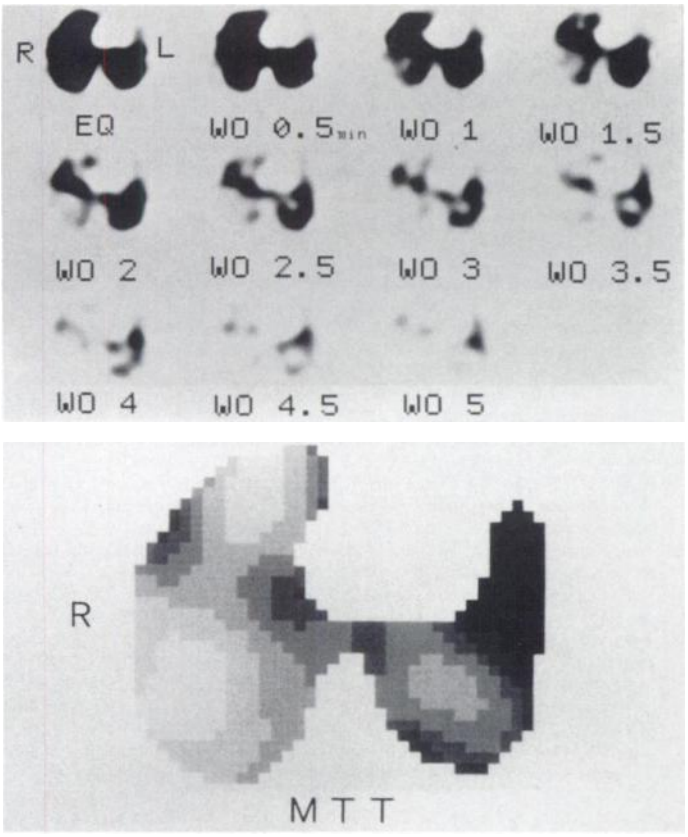

FIGURE 4. SPECT image from a 59-yr-old woman with bronchial asthma shows heterogeneous ^{133}Xe retention in both lungs (top). Chest CT scan does not show any abnormalities. MTT image shows heterogeneously prolonged MTT in both lungs (bottom).

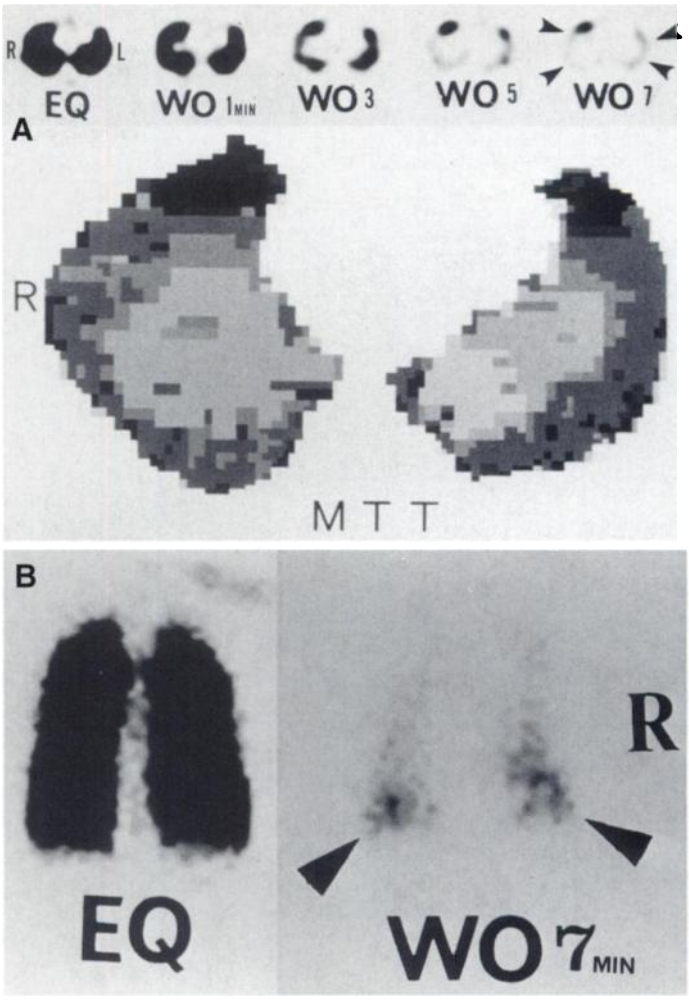

FIGURE 5. (A) SPECT image from a 35-yr-old man with DPB shows marked ^{133}Xe retention in ventral portions in lower lung, and characteristic, symmetrical retention in both outer lung zones (arrowheads) (top). Chest CT scan shows scattered centrilobular tiny nodules in both middle and lower lobes. MTT image shows prolonged MTT in outer zones (bottom). (B) Planar image shows retention in lower lungs (arrowheads), but characteristic retention in outer zones cannot be recognized.

washout delay in lung regions without abnormal retention, as noted in the obstructive lung diseases. Quantitative accuracy of SPECT, in which retention sites and well-ventilated lungs can be distinguished on cross-section imaging, is considered to be greater than a planar study because in a planar study ^{133}Xe washout at the retention site is influenced by fast washout of the overlapped well-ventilated lungs (*1–4,7*). The greater $T_{1/2}$ in the abnormal lung regions with ^{133}Xe retention in the SPECT rather than planar study indicates that SPECT can eliminate the influence of the overlapped lungs having faster washout. The greater difference in $T_{1/2}$ between these lung regions and normal lungs on SPECT images suggests that this modality is more sensitive for detecting abnormal ventilation sites than the planar study.

On the other hand, the comparison of the summed coronal SPECT and planar studies showed longer $T_{1/2}$ in SPECT study than in planar study (Table 1). In CRRA mode, averaging together projection data from similar angles obtained at different time points does not eliminate all effects of ^{133}Xe washout for the duration between the two time points (*20,21*). Prolonged $T_{1/2}$ may be caused by a rapid change in ^{133}Xe activity during image acquisition. To obtain a more accurate $T_{1/2}$, more rapid data acquisition sensitive to fast washout times may be necessary. Our comparative study, however, revealed high correlation in $T_{1/2}$ between SPECT and planar studies (Fig. 6), indicating that a quantitative approach is applicable to SPECT despite the difference in absolute $T_{1/2}$ between the two studies.

Until now, tomographic imaging of pulmonary washout of radioactive gas has been performed only with PET with ^{13}N-labeled nitrogen gas (*13,14,17*). PET demonstrated the gravitational effect of ventilation in normal lungs, a characteristic outer lung zone's washout delay in a DPB patient and a lack of washout delay in patients with restrictive lung disease. These findings are similar to our results. The PET study is not yet a routine procedure, probably due to its complexity, limited availability of the gas and the prohibitive costs. In contrast, ^{133}Xe gas is widely available (*1–12*), and the CRRA mode has been widely equipped in recent multidetector SPECT system (*20,21*).

TABLE 3
Comparison of $T_{1/2}$ among Subjects and Patients with Obstructive and Restrictive Lung Diseases

Subjects	Mean $T_{1/2}$ ± s.d. (sec)
Healthy volunteers (n = 7)	48.4 ± 4.3
Obstructive lung disease (n = 22)	114.6 ± 26.4*
^{133}Xe retention sites	(136.2 ± 37.8)
Nonretention sites	(84.5 ± 14.2)
Restrictive lung disease (n = 10)	56.8 ± 3.9†
Affected lung areas	(56.4 ± 4.2)
Unaffected lung areas	(57.3 ± 3.7)

*Combined $T_{1/2}$ value for ^{133}Xe retention and nonretention sites.
†Combined $T_{1/2}$ value for affected and unaffected lung sites.

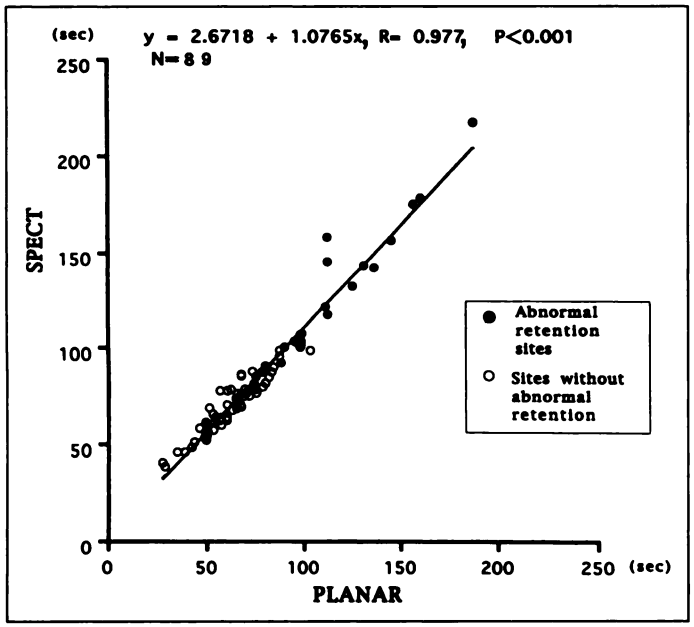

FIGURE 6. Comparison of $T_{1/2}$ between planar and summed coronal SPECT images in 19 patients.

CONCLUSION

Dynamic SPECT with ^{133}Xe appears to have excellent potential to elucidate the nature of ventilation abnormalities. Compared to the planar study, this modality seems to be spatially superior and more sensitive for detecting ventilatory abnormalities. A quantitative approach using the $T_{1/2}$ appears applicable to SPECT because there was high correlation with the planar study. A functional MTT image is also useful in depicting heterogeneous distribution of ^{133}Xe washout.

REFERENCES

1. Alderson PO, Line BR. Scintigraphic evaluation of regional pulmonary ventilation. *Semin Nucl Med* 1980;10:218–242.
2. Ball WC, Stewart PB, Newshaw LGS. Regional pulmonary function studies with Xenon-133. *J Clin Invest* 1962;41:519–531.
3. Bunow B, Line BR, Horton MR, Weiss GH. Regional ventilatory clearance by xenon scintigraphy: a critical evaluation of two estimation procedure. *J Nucl Med* 1979;20: 703–710.
4. Van der Mark TW, Peset R, Beekhuis H. An improved method for analysis of ^{133}Xe washin and washout curves. *J Nucl Med* 1980;21:1029–1034.
5. Peset R, Holloway R, Beekhuis K. Ventilation and perfusion indices measured with xenon-133 during spontaneous breathing. *Radioact Isot Clin Med Res* 1970;9:266–275.
6. Schor RA, Shames DM, Weber PM, Dos Remedios LV. Regional ventilation studies with ^{81m}Kr and ^{133}Xe: a comparative analysis. *J Nucl Med* 1978;19:348–353.
7. Secker-Walker RH, Hill RI, Markham J. The measurement of regional ventilation in man: a new method of quantitation. *J Nucl Med* 1973;14:725–732.
8. Alderson PO, Lee H, Summer WR, Motazedi A, Wagner HN. Comparison of ^{133}Xe washout and single-breath imaging for the detection of ventilation abnormalities. *J Nucl Med* 1979;20:917–922.
9. Alderson PO, Secker-Walker RH, Forrest JV. Detection of obstructive pulmonary disease. Relative sensitivity of ventilation-perfusion studies and chest radiography. *Radiology* 1974;111:643–648.
10. Suskind H, Atkins HL, Goldman AG, et al. Sensitivity of ^{81m}Kr and ^{127}Xe in evaluating nonembolic pulmonary disease. *J Nucl Med* 1981;22:781–786.
11. Ishii Y, Itoh H, Suzuki T, Yonekura Y, Mukai T, Torizuka K. Quantitative assessment of ventilation-perfusion mismatch by radioxenon imaging of the lung. *J Nucl Med* 1978;19:607–614.
12. Dittrich FA, Goodwin DA. Early recognition of chronic airway disease by the ^{133}Xe lung scan. *JAMA* 1972;220:1120–1122.
13. Senda M, Murata K, Ito H, et al. Quantitative evaluation of regional pulmonary ventilation using PET and nitrogen-13 gas. *J Nucl Med* 1986;27:268–273.
14. Murata K, Itoh H, Senda M, et al. Ventilation imaging with positron emission tomography and nitrogen-13. *Radiology* 1986;158:303–307.
15. Ramos M, Baumann HR, Muhlberger F. Perfusion and ventilation imaging in pulmonary tuberculosis. *Clin Nucl Med* 1978;3:233–242.
16. Mark ThW, Rookmaker AEC, Kiers A, et al. Nitrogen-13 and xenon-133 ventilation studies. *J Nucl Med* 1984;25:1175–1182.
17. Valind SO, Rhodes CG, Brudin LH, Jones T. Measurements of regional ventilation pulmonary gas volume: theory and error analysis with special reference to positron emission tomography. *J Nucl Med* 1991;32:1937–1944.
18. Lavender JP, Al-Nahhas AM, Myers MJ. Ventilation perfusion ratios of the normal supine lung using emission tomography. *Br J Radiol* 1984;57:141–146.
19. Osborne DRS, Jazczak R, Coleman RE. Single-photon emission computed tomography and its application in the lung. *Radiol Clin North Am* 1983;21:789–800.
20. Nakajima K, Shuke N, Taki J, et al. A simulation of dynamic SPECT using radiopharmaceuticals with rapid clearance. *J Nucl Med* 1992;33:1200–1206.
21. Nakajima K, Taki T, Iwasaki Y, et al. Dynamic acquisition with a three-headed SPECT system: application to technetium-99m-SQ 30217 myocardial imaging. *J Nucl Med* 1991;32:1273–1277.
22. Kouris K, Clarke GA, Jarritt PH, Townsend CE, Thomas SN. Physical performance evaluation of the Toshiba GCA-9300 A triple-headed system. *J Nucl Med* 1993;34: 1778–1789.
23. Bok BD, Bice AN, Clausen M, Wong DF, Wagner Jr HN. Artifacts in camera-based single-photon emission tomography due to time activity variation. *Eur J Nucl Med* 1987;13:439–442.
24. Links JM, Frank TL, Becker LC. Effect of differential tracer washout during SPECT acquisition. *J Nucl Med* 1991;32:2253–2257.
25. Yonekura Y, Mukai T, Iwasaki Y, et al. Kinetic analysis of N-isopropyl-p-iodoamphetamine in human brain [Abstract]. *J Nucl Med* 1991;32(suppl):991P.
26. Chiao P, Rogers WL, Clinthorne NH, Hutchinns GD. Optimal dynamic SPECT data acquisition protocols for myocardial blood flow studies [Abstract]. *J Nucl Med* 1990;31(suppl):718.
27. Budinger T, Araujo L, Ranger N, et al. Dynamic SPECT feasibility studies [Abstract]. *J Nucl Med* 1991;32(suppl):955.
28. Maeda H, Takeda K, Matsumura K, et al. The influence of the time activity variation on Dynamic SPECT images in camera-based SPECT. *Jpn J Nucl Med* 1991;28:27–34.
29. Secker-Walker RH, Hill RI, Markham J, et al. The measurement of regional ventilation in man: a new method of quantitation. *J Nucl Med* 1973;14:725–732.
30. Alpert NM, McKusick KA, Correia JA, Shea W, Brownell GL, Potsaid MS. Initial assessment of a simple image of ventilation. *J Nucl Med* 1975;17:88–92.
31. Webb WR, Stern EJ, Kanth N, Gamsu G. Dynamic pulmonary CT: findings in healthy adult men. *Radiology* 1993;186:117–124.
32. Archer DC, Coblentz CL, DeKemp RA, Nahmias MC, Norman G. Automated in vivo quantification of emphysema. *Radiology* 1993;188:835–838.
33. Reid L, Millard FJ. Correlation between radiological diagnosis and structural lung changes in emphysema. *Radiology* 1964;15:307–311.
34. Homma H, Yamanaka A, Tanimoto S, et al. Diffuse panbronchiolitis: a disease of the transitional zone of the lung. *Chest* 1983;83:63–69.